Low-Complexity Superresolution Frequency Offset Estimation for High Data Rate Acoustic OFDM Systems

Amir Tadayon, *Graduate Student Member, IEEE*, and Milica Stojanovic, *Fellow, IEEE*

***Abstract*—This paper addresses the problem of compensating for motion-induced Doppler frequency offset in multicarrier acoustic communication systems based on orthogonal frequency-division multiplexing (OFDM). In mobile acoustic systems, Doppler effect can be severe enough that the received OFDM signal experiences nonnegligible frequency offsets even after initial resampling. To target these offsets, a superresolution, yet low-complexity method based on a stochastic gradient approach is proposed. The method relies on differentially coherent detection that keeps the receiver complexity at a minimum and requires only a small pilot overhead. Differential encoding is applied across carriers, promoting the use of a large number of closely spaced carriers within a given bandwidth. This approach simultaneously supports frequency-domain coherence and efficient use of bandwidth for achieving high bit rates. While frequency synchronization capitalizes on differentially coherent detection, it can also be used as a preprocessing stage in coherent receivers without creating undue complexity. Using simulation, as well as the experimental data transmitted over a 3–7-km shallow-water channel in the 10.5–15.5-kHz acoustic band, we study the system performance in terms of data detection mean squared error and bit error rate, and show that the proposed method provides excellent performance at low computational cost. Such advantages are of paramount importance for practical implementation of high data rate acoustic OFDM systems.**

***Index Terms*—Frequency offset estimation, orthogonal frequency-division multiplexing (OFDM), underwater acoustic (UWA) communications.**

I. Introduction

THE fundamental obstacle to robust underwater acoustic (UWA) communications is the combined effects of long multipath and Doppler fluctuations. Orthogonal frequency-division multiplexing (OFDM) offers remarkable robustness against frequency-selective channels at reasonably low computational loads. This fact motivates the use of OFDM in mobile acoustic communications where the channel exhibits long multipath delays but each narrowband carrier only experiences flat fading, thus eliminating the need for time-domain equalizers [1]–[5].

Manuscript received January 18, 2018; revised May 20, 2018 and July 29, 2018; accepted September 5, 2018. This work was supported in part by under Grant ONR N00014-15-1-2550, under Grant NSF CNS-1726512, and under Grant NSF 1428567. *(Corresponding author: Amir Tadayon.)*

Guest Editor: A. Sen Gupta.

The authors are with the Northeastern University, Boston, MA 02115 USA (e-mail: amir.tadayon@gmail.com; millitsa@ece.neu.edu).

Digital Object Identifier 10.1109/JOE.2018.2869657

The major problem in applying OFDM to acoustic channels is the Doppler distortion caused by relative motion between the transmitter and receiver, which results in frequency shifting. For the relative transmitter/receiver velocity v and the propagation speed c (nominally 1500 m/s), Doppler scaling occurs at the rate $a = v/c$. In highly mobile scenarios, where v is on the order of a few meter per second, Doppler frequency scaling is effectively seen as a time-varying channel distortion that adversely affects the performance of OFDM systems as it causes loss of orthogonality between the carriers. To mitigate the resulting distortion, front-end resampling must be performed [3]–[5]. Coarse resampling is typically performed on an entire frame of OFDM blocks, and may leave individual blocks within a frame exposed to different frequency offsets. A residual carrier frequency offsets (CFOs) destroys the orthogonality among carriers, thus causing two detrimental effects, namely reduction in the signal-to-noise ratio (SNR) at the output of the filters matched to each carrier, and intercarrier interference. As a result, the bit error rate (BER) performance is severely degraded [6], [7]. Therefore, OFDM for UWA communications requires agile and accurate estimation of CFO. In this paper, we target estimation of residual CFO within a single block of an OFDM system.

The extensive literature on CFO estimation for OFDM can be categorized into data-aided schemes and nondata-aided (blind) schemes. The data-aided schemes (e.g., [7] and [8]) rely on the periodic transmission of known OFDM blocks. Moose in [7] presented the maximum likelihood (ML) estimator for the CFO, which is calculated in the frequency domain after fast Fourier transform (FFT) demodulation. This technique relies on transmission of two consecutive and identical OFDM blocks and is based on the assumption that the channel remains unchanged for the duration of the two blocks. Schmidl and Cox [8] proposed a two-step method through the use of a two-block training sequence that doubles the acquisition range compared to the method in [7]. In this technique, after finding the frame timing by searching for a block in which the first half is identical to the second half in the time domain, the CFO is partially corrected and a correlation with the second block is performed to find the CFO.

The data-aided methods assume that the frequency offset is time-invariant for the duration of a number of OFDM blocks. Moreover, due to the transmission of known sequences, these techniques incur a loss in the information rate. To avoid this loss and target time-varying frequency offsets, a blind method

that exploits only the specific redundancy offered by the presence of cyclic prefix (CP) was proposed in [9]. The basic idea underlying [9] is that on ideal channels, the first and last sample of each OFDM block are equal to each other. More specifically, Van de Beek *et al.* [9] proved that their method approximates the optimum ML estimator when the channel is ideal. However, the performance of the method degrades considerably as frequency selectivity becomes more pronounced, and as shown in [9], the variance of the carrier offset estimate exhibits a floor at high SNR.

In this paper, we propose a method that targets time-varying CFO for acoustic channels with long multipath and severe Doppler fluctuations based on a stochastic gradient (SG) approach. Unlike the CP-based method [9], this method can also be used in acoustic OFDM systems which adopt zero-padding to save transmission power over long guard intervals. In addition, the proposed method has the capability of exploiting spatial diversity to obtain a better estimate of the CFO. The method is based on differentially coherent detection that keeps the receiver complexity at a minimum and requires only a very low pilot overhead. Differential encoding is applied across carriers, promoting the use of a large number of carriers within a given bandwidth [5], and offering a computationally efficient alternative to differentially coherent detection in single-carrier systems [10], [11]. While narrow carrier spacing ensures frequency-domain coherence, it simultaneously supports efficient use of bandwidth for achieving high bit rates. The method can be deemed as an adaptive version of the hypothesis testing (HT) approach presented in [12], with more accurate estimation of CFO that results in an improved mean squared error (MSE) performance at significantly lower computational cost.

The technique is demonstrated on both simulated data and experimental data from the Mobile Acoustic Communication Experiment (MACE'10), showing excellent results in situations with Doppler frequency offsets on the order of a carrier spacing. In the MACE'10 experiment, the transmitter moved at a relative speed of 0.5–1.5 m/s with respect to the receiver, and OFDM blocks containing up to 2048 carriers which conveyed QPSK/8 phase shift keying (8-PSK) data symbols and occupied the acoustic frequency range between 10.5 and 15.5 kHz. The proposed method achieves excellent performance in these challenging conditions.

The rest of this paper is organized as follows. In Section II, we introduce the signal and system model. Section III briefly discusses the hypothesis-based approach and details the proposed method for compensating frequency offsets. Section IV and Section V contain the results of simulation and experimental data processing, respectively. Conclusions are summarized in Section VI.

II. Signal and System Model

We consider an OFDM system with M_r equispaced receivers and K carriers within a total bandwidth B. Let f_0 and $\Delta f = B/K$ denote the first carrier frequency and carrier spacing, respectively. We assume the use of zero-padding at the transmitter along with the overlap-and-add procedure at the receiver [13]. The transmitted OFDM block is then given by

$$s(t) = Re\left\{\sum_{k=0}^{K-1} d_k e^{2\pi i f_k t}\right\}, \quad t \in [0, T] \tag{1}$$

where $T = 1/\Delta f$ is the OFDM block duration. The data symbol d_k, which modulates the kth carrier of frequency $f_k = f_0 + k\Delta f$, belongs to a unit-amplitude PSK alphabet.

The transmitted signal passes through a multipath acoustic channel whose impulse response can be modeled as follows:

$$h(\tau, t) = \sum_p h_p(t)\delta(\tau - \tau_p(t)) \tag{2}$$

where $h_p(t)$ and $\tau_p(t)$ represent the gain and delay of the pth path, respectively. We isolate a common Doppler scaling factor a such that $\tau_p(t) \approx \tau_p - at$, and further assume that the path gains are slowly varying such that $h_p(t) \approx h_p$ for the duration of one OFDM block. With these notions, we can rewrite (2) as follows:

$$h(\tau, t) \approx \sum_p h_p \delta(\tau - \tau_p + at). \tag{3}$$

After frame synchronization, initial resampling and downconversion, the lowpass equivalent received signal on the mth receiving element is modeled as follows:

$$v_m(t) = e^{i\beta t} \sum_{k=0}^{K-1} H_k^m d_k e^{2\pi i k \Delta f t} + w_m(t), \quad t \in [0, T] \tag{4}$$

where β is the unknown frequency offset assumed common for all M_r receiving elements, H_k^m is the channel frequency response on the kth carrier of the mth receiving elements, and $w_m(t)$ is the additive complex Gaussian noise, assumed to be uncorrelated between the receiving elements. Assuming the same gross frequency offset β for all receiving elements is plausible when the elements are colocated, and it helps to promote the multichannel processing gain.

The model (4) captures rough frequency shifting and serves as a starting point in developing the method for frequency offset compensation. The finer points of frequency shift changing across the bandwidth are left to post-FFT processing.

III. Frequency Offset Estimation

A. Hypothesis Testing (HT) Approach

In this approach, several hypothesized values of the frequency offset are used, e.g., with resolution of $\Delta f/10$, and differential maximal ratio combining (DMRC) is performed for each hypothesized value. Specifically, let us assume that the M_r signals are compensated by some hypothesized value $\hat{\beta}$, and that demodulation is performed on all the receiving elements to yield

$$y_k^m = \int_T v_m(t) e^{-i\hat{\beta}t} e^{-2\pi i k \Delta f t} dt \tag{5}$$

where $k = 0, \ldots, K-1$ and $m = 1, \ldots, M_r$. Arranging the signals corresponding to carrier k into a vector $\mathbf{y}_k$ and performing DMRC, the estimates of the differentially decoded data

symbols $b_k = d_{k-1}^* d_k$ are obtained as[1]

$$\hat{b}_k = \frac{\sum_{m=1}^{M_r} (y_{k-1}^m)^* y_k^m}{\sum_{m=1}^{M_r} (y_{k-1}^m)^* y_{k-1}^m} = \frac{1}{\mathbf{y}_{k-1}^H \mathbf{y}_{k-1}} \mathbf{y}_{k-1}^H \mathbf{y}_k = \mathbf{a}_k^H \mathbf{y}_k. \tag{6}$$

Here, we implicitly assume that the channel frequency response changes slowly from one carrier to the next, i.e., $H_{k-1}^m \approx H_k^m \quad \forall k = 1, \ldots, K-1$ and $m = 1, \ldots, M_r$ [5].

Using equally spaced pilot data symbols $b_k, k \in \mathcal{K}_p$, where $\mathcal{K}_p$ is the set of pilot carriers, the composite squared error is formed as follows:

$$E(\hat{\beta}) = \sum_{k \in \mathcal{K}_p} |b_k - \hat{b}_k|^2 \tag{7}$$

and the estimate $\hat{\beta}^\star$ is obtained as $\hat{\beta}^\star = \arg\min_{\hat{\beta}} E(\hat{\beta})$.

B. Stochastic Gradient (SG) Approach

The finite resolution of the frequency offset estimate obtained from the HT approach gives rise to an error floor in the estimator variance. To reduce the variance of the estimate, we develop an SG approach where the composite squared error (7) is used to close the loop and guide the estimation of β.[2]

To gain insight into the operation of the SG loop, let us assume for the moment that the DMRC coefficients $\mathbf{a}_k$ are fixed. This type of assumption is often used in developing adaptive algorithms in the context of differentially coherent detection [11]. With $\mathbf{a}_k$ independent of β, the gradient of the composite squared error is given by

$$\frac{\partial E(\hat{\beta})}{\partial \hat{\beta}} = -2Im \left\{ \sum_{k \in \mathcal{K}_p} \mathbf{a}_k^H \tilde{\mathbf{y}}_k e_k^* \right\} \tag{8}$$

where $e_k = b_k - \hat{b}_k \quad \forall k \in \mathcal{K}_p$ and the mth element of $\tilde{\mathbf{y}}_k$ is given by

$$\tilde{y}_k^m = \int_T t v_m(t) e^{-i\hat{\beta}t} e^{-2\pi i k \Delta f t} dt, \quad m = 0, \ldots, M_r. \tag{9}$$

Using the gradient, $\hat{\beta}$ can be calculated iteratively as follows:

$$\hat{\beta}(j+1) = \hat{\beta}(j) + K_\beta \gamma(j), \quad j \geq 0 \tag{10}$$

where $\gamma(j) = Im\{\sum_{k \in \mathcal{K}_p} \mathbf{a}_k^H(j) \tilde{\mathbf{y}}_k(j) e_k^*(j)\}$, and K_β is the frequency offset update parameter. The initial point $\hat{\beta}(0)$ can be set to zero when the frequency offset $\beta/2\pi$ is a fraction of carrier spacing Δf. We will comment on the initial point and step size later. In each iteration, $y_k^m(j)$ and $\tilde{y}_k^m(j)$ can be obtained using FFT, applied to the samples of $v_m(t)$ and $t v_m(t)$, respectively.

In deriving (8), we naively ignored the fact that once the loop is closed, the DMRC coefficients $\mathbf{a}_k$ will be computed from the input signals $\mathbf{y}_k$, and will, hence, depend on the offset β. Taking into account the dependence of $\mathbf{a}_k$ on β, we obtain an alternative approach resulting in better MSE performance. To arrive at this algorithm, we define the following:

$$p_k = \mathbf{y}_{k-1}^H \mathbf{y}_k \tag{11a}$$

$$q_k = \mathbf{y}_{k-1}^H \mathbf{y}_{k-1} \tag{11b}$$

$$\tilde{p}_k = \mathbf{y}_{k-1}^H \tilde{\mathbf{y}}_k - \tilde{\mathbf{y}}_{k-1}^H \mathbf{y}_k \tag{11c}$$

$$\tilde{q}_k = \mathbf{y}_{k-1}^H \tilde{\mathbf{y}}_{k-1} - \tilde{\mathbf{y}}_{k-1}^H \mathbf{y}_{k-1} \tag{11d}$$

where $\tilde{p}_k = i(\partial p_k / \partial \hat{\beta})$ and $\tilde{q}_k = i(\partial q_k / \partial \hat{\beta})$. With these definitions, the estimate of the differentially decoded data symbols is obtained as follows:

$$\hat{b}_k = \frac{p_k}{q_k}. \tag{12}$$

The gradient of the composite squared error is then given by

$$\frac{\partial E(\hat{\beta})}{\partial \hat{\beta}} = -2 \underbrace{Im \left\{ \sum_{k \in \mathcal{K}_p} \frac{1}{q_k} \left[\tilde{p}_k - \tilde{q}_k \hat{b}_k \right] e_k^* \right\}}_{\gamma}. \tag{13}$$

SG recursion remains as in (10), with the increment γ defined in (13). While gradient descent is a classical tool used in many algorithms that target frequency offset estimation, e.g., [14] and [15], here it is tailored for differentially coherent detection, and also exploits spatial diversity to compensate for the frequency offset before FFT demodulation. The algorithm can be set to run either for a prespecified maximum number of iterations N_I or a predefined error threshold η. Fig. 1 shows the block diagram of the SG algorithm.

Fig. 2 shows the composite squared error (7). Although this error has a global minimum, it is a nonconvex function of the frequency offset $\hat{\beta}$ [or equivalently, the normalized frequency offset $\hat{\epsilon} = (\hat{\beta}/2\pi\Delta f)$]. Thus, if the initial point $\hat{\beta}(0)$ is not properly selected, the SG algorithm may converge to a local minimum. To address this issue in block-by-block receivers, we use the HT approach as an acquisition technique that can operate with an arbitrary range of hypothesized frequency offsets to compensate for the frequency offset in the first block. Capitalizing on the fact the frequency offset from one block to the next is not changing significantly, from the second block and on, we employ the SG approach where the initial value $\hat{\beta}(0)$ is set to the frequency offset estimated in the previous block. We use this approach to process the real data obtained from the MACE'10 experiment (see Section V).

In addition to properly specifying the initial point, careful selection of the step size is often necessary to obtain good performance from the SG algorithm. The step size has a notable impact on the convergence speed of the algorithm. To improve the convergence speed, we use the Barzilai–Borwein (BB) method proposed in [16] to update the step size. In the BB method, the step size is derived from a two-point approximation to the secant equation underlying quasi-Newton methods as follows:

$$K_\beta(j) = \frac{\hat{\beta}(j) - \hat{\beta}(j-1)}{2(\gamma(j-1) - \gamma(j))} \approx \left(\frac{\partial^2 E(\hat{\beta})}{\partial \hat{\beta}^2} \right)^{-1}. \tag{14}$$

[1] $(\cdot)^*$ and $(\cdot)^H$ denote complex conjugate and Hermitian transpose, respectively.

[2] Note that this type of algorithm is sometimes also referred to as steepest descent in the optimization theory.

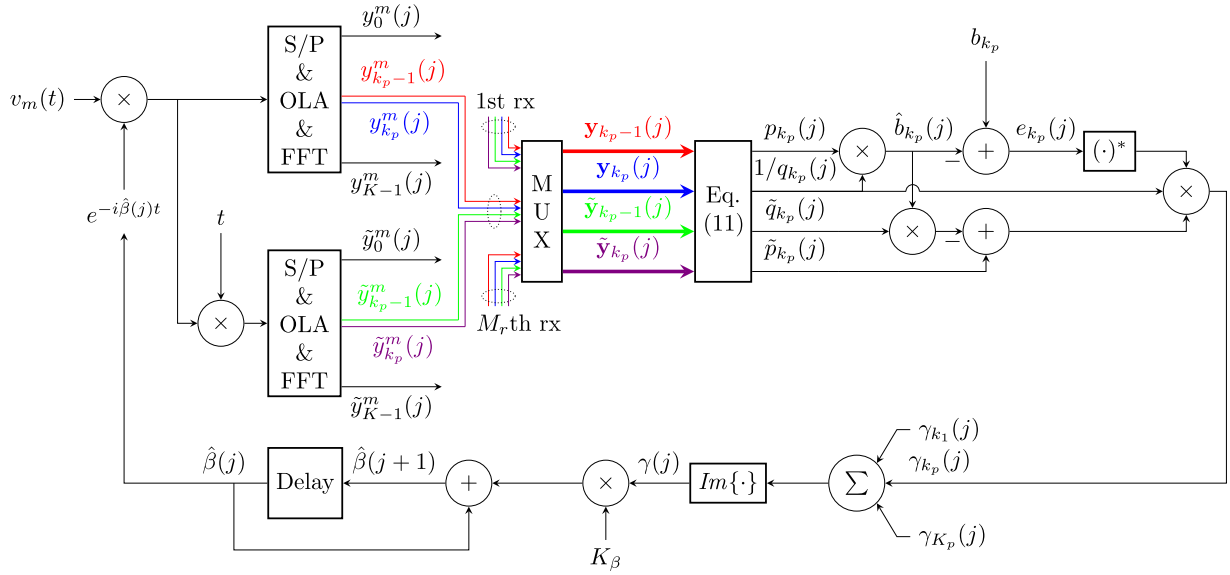

Fig. 1. Block diagram of SG algorithm for a ZP-OFDM system with multiple receiving elements.

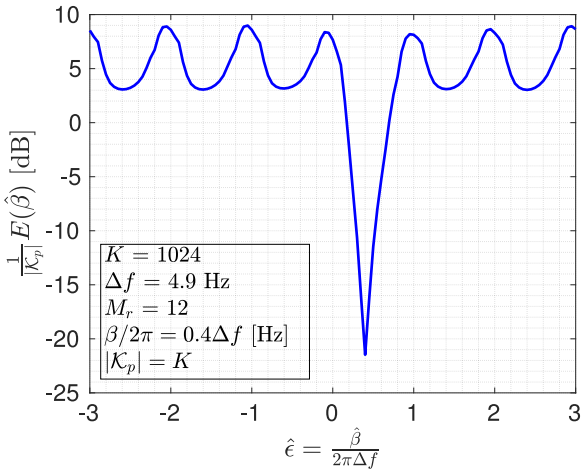

Fig. 2. Normalized composite squared error $(1/|\mathcal{K}_p|)E(\hat{\beta})$ for a ZP-OFDM block with $K = 1024$ and $\Delta f = 4.9$ Hz. The actual frequency offset is set to $\beta/2\pi = 0.4\Delta f$. The composite squared error is a nonconvex function of frequency offset $\hat{\beta} = 2\pi\hat{\epsilon}\Delta f$.

For the iteration $j = 0$ where $\hat{\beta}(-1)$ and $\gamma(-1)$ are unavailable, $K_\beta(0)$ is set to a small value to preclude the algorithm from diverging.

The formal steps of the SG algorithm are summarized in Algorithm 1. The computational cost of the algorithm is primarily dominated by steps (3) and (4), which take $O(2M_r K \log(K))$ operations per iteration due to FFT computation. The operations in the other steps of the algorithm require a total $|\mathcal{K}_p|(12M_r + 2)$ of complex multiplications, additions, and divisions per iteration. For practical systems where $K \gg |\mathcal{K}_p|$, the total cost of the algorithm is upper-bounded by $O(2N_I M_r K \log(K))$, where N_I is the maximum number of iterations.

Algorithm 1: SG Algorithm With BB Step Size.

Input: $\mathbf{v}(t) = [v_1(t) \ \cdots \ v_{M_r}(t)]^T$, set of pilot carriers $\mathcal{K}_p$,
pilot data symbols b_k $(\forall k \in \mathcal{K}_p)$, N_I, η, $K_\beta(0)$, and $\hat{\beta}(0)$

Output: $\hat{\beta}^\star$

$j = 0$ and $E(\hat{\beta}; -1) = 0$
while $(j \leq N_I)$ **do**
  $\mathbf{y}_k(j) = \int_T \mathbf{v}(t) e^{-i\hat{\beta}(j)t} e^{-2\pi i k \Delta f t} dt, \forall k$
  $\tilde{\mathbf{y}}_k(j) = \int_T t\mathbf{v}(t) e^{-i\hat{\beta}(j)t} e^{-2\pi i k \Delta f t} dt, \forall k$
  for $k \in \mathcal{K}_p$ **do**
    $p_k(j) = \mathbf{y}_{k-1}^H(j)\mathbf{y}_k(j)$, $q_k(j) = \mathbf{y}_{k-1}^H(j)\mathbf{y}_{k-1}(j)$
    $\tilde{p}_k(j) = \mathbf{y}_{k-1}^H(j)\tilde{\mathbf{y}}_k(j) - \tilde{\mathbf{y}}_{k-1}^H(j)\mathbf{y}_k(j)$
    $\tilde{q}_k(j) = \mathbf{y}_{k-1}^H(j)\tilde{\mathbf{y}}_{k-1}(j) - \tilde{\mathbf{y}}_{k-1}^H(i)\mathbf{y}_{k-1}(j)$
    $\hat{b}_k(j) = \frac{p_k(j)}{q_k(j)}$, $e_k(j) = b_k - \hat{b}_k(j)$
    $\gamma_k(j) = \frac{1}{q_k(j)} \left[\tilde{p}_k(j) - \tilde{q}_k(j)\hat{b}_k(j)\right] e_k^*(i)$
  end for
  $E(\hat{\beta}; j) = \sum_{k \in \mathcal{K}_p} |e_k(j)|^2$
  if $(|10\log_{10}(\frac{E(\hat{\beta};j)}{E(\hat{\beta},j-1)})| > \eta)$ **then**
    $\gamma(j) = Im\left\{\sum_{k \in \mathcal{K}_p} \gamma_k(j)\right\}$
    if $(j > 0)$ **then**
      $K_\beta(j) = \frac{\hat{\beta}(j) - \hat{\beta}(j-1)}{2(\gamma(j-1) - \gamma(j))}$
    end if
    $\hat{\beta}(j+1) = \hat{\beta}(j) + K_\beta(j)\gamma(j)$
  else
    break
  end if
  $j = j + 1$
end while
return $\hat{\beta}^\star = \hat{\beta}(j)$

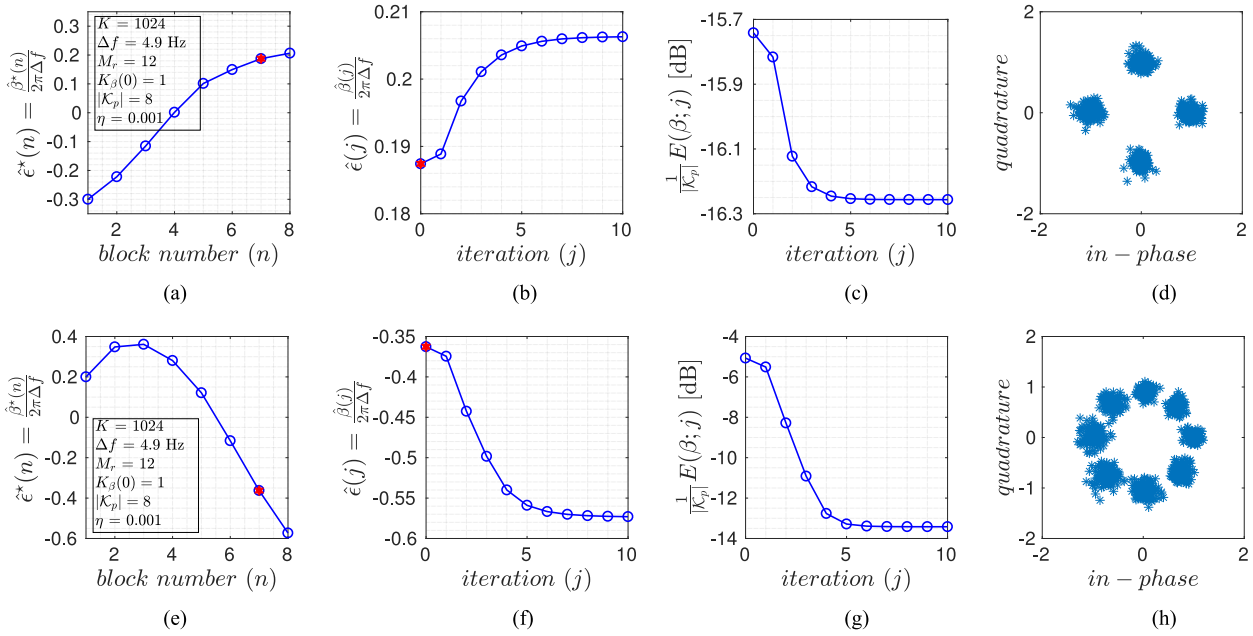

Fig. 3. Performance illustration for an OFDM frame with 8 blocks and $K = 1024$ carriers modulated by differentially encoded QPSK (*top*) and 8-PSK (*bottom*) data symbols. Shown are the normalized frequency offset estimate (NFOE) for the entire frame, the evolution of the frequency offset estimate for the last block, the algorithm convergence plot obtained for the last block, and the last block.s scatter plot. Only 8 pilots are used and the initial value of K_β is set to 1. hypothesis testing approach is applied to the first block to perform the acquisition step. For the second block and on, the initial value of the update (13) is set to the frequency offset estimated in the previous block [colored circles in (a), (b), (e), and (f)]. In the scatter plots shown in (d) and (h), the data detection MSE is -17.5 dB and -15.3 dB, respectively, and there are no symbols errors. (a) and (e) NFOE. (b) and (f) Evolution of NFOE. (c) and (g) Convergence plot. (d) and (h) Scatter plot.

In Fig. 3, we illustrate the algorithm operation on two OFDM frames of experimental recordings, one carrying QPSK data and the other 8-PSK. Each frame has eight blocks and $K = 1024$ carriers. The normalized frequency offset estimate for the eight blocks in the underlying frames, the algorithm convergence plot obtained for the last block of each frame, the evolution of the frequency offset estimate for the last block, and the last block's scatter plot are shown.

IV. Simulation Results

In this section, we assess the performance of the proposed SG frequency offset estimator through simulation and compare it to that of the HT approach. We report on the performance of the two variants of the SG algorithm, one based on (8) and the other based on (13), and the HT method in terms of the data detection MSE and the normalized standard deviation of the estimation error.

In the simulation, one OFDM block with $K = 1024$ carriers modulated by data symbols from the QPSK constellation is transmitted through a synthetic UWA channel. We utilize the statistical channel model proposed in [17] to simulate the UWA channel and choose the channel geometry parameters corresponding to those in the MACE'10 experiment. The receiver uses a vertical array with four equally spaced receiving elements that are spaced $d_{\text{rx}} = 12$ cm apart. We assume that the propagation time across the array is short compared to the block duration, i.e., that each receiving element sees the same basic multipath structure. The channel path delays seen by the mth element are modeled as follows:

$$\tau_p^{(m)} = \tau_p^{(1)} + (m-1)\frac{d_{\text{rx}}}{c}\sin(\theta_p) \tag{15}$$

where θ_p is the angle of arrival of the pth channel path with respect to the broadside of the receiver array. The complex Gaussian channel path amplitudes h_p seen by the receiving elements are generated independently. The average energy of the channel impulse response is normalized to unity. Table I summarizes the simulation parameters.

Fig. 4(a) illustrates the performance of the HT and SG approaches in terms of data detection MSE as a function of the SNR at the input to the algorithm. The MSE is measured as follows:

$$\text{MSE} = \frac{1}{N_r}\sum_{i=1}^{N_r}\frac{1}{K-1}\sum_{k=1}^{K-1}|b_k^i - \hat{b}_k^i|^2 \tag{16}$$

where $\hat{b}_k^i$ is the estimate of the kth differentially encoded data symbol b_k^i in the ith realization and N_r is the number of channel and noise realizations. Clearly, the SG method based on (13) outperforms the method where the gradient is given by (8) at negligible computational burden [$|\mathcal{K}_p|(12M_r + 2)$ operations, twice the number needed by (8)]. Hence, in the rest of the analysis, we will focus on the performance of the SG algorithm based on (13). The SG method also shows superior performance compared to the HT algorithm, which it achieves by virtue of superresolution frequency offset estimation. This fact is quantified in Fig. 4(b), which shows the root normalized MSE of the

TABLE I
SIMULATION PARAMETERS

water depth [m]	100	bandwidth B [kHz]	5
distance between tx and rx [km]	3	lowest carrier frequency f_0 [kHz]	10.5
transmitter depth [m]	55	number of carriers K	1024
receiver depth [m]	40	carrier spacing Δf [Hz]	4.9

The distance between receiving elements is $d_{\text{rx}} = 12$ cm. The frequency offset is $\beta/2\pi = 0.12\Delta f$ Hz and the guard interval is $T_g = 16$ ms. The number of pilots is $|\mathcal{K}_p| = 8$.

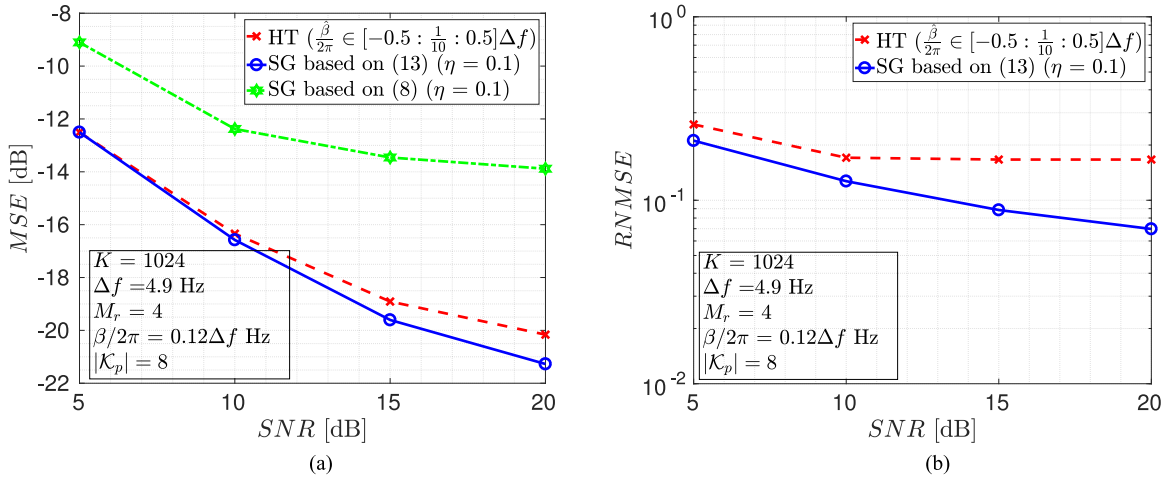

Fig. 4. Performance of the HT and SG algorithms for 20 000 realizations of the MACE'10-like simulated UWA channel. (a) MSE of data detection and (b) normalized standard deviation of the estimate as functions of the SNR at the input to the receiver are shown. The actual frequency offset is $\beta/2\pi = 0.12\Delta f$. Only eight pilots are used and the hypothesized values range from $-0.5\Delta f$ to $0.5\Delta f$ in steps of $\Delta f/10$.

estimators given by

$$\text{RNMSE} = \frac{\sqrt{\frac{1}{N_r}\sum_{i=1}^{N_r}(\beta - \hat{\beta}_i^{\star})^2}}{\beta} \tag{17}$$

where $\hat{\beta}_i^{\star}$ is the estimate of the frequency offset β in the ith realization.

V. EXPERIMENTAL RESULTS

In this section, we provide the results from the MACE'10 which took place off the coast of Martha's Vineyard, MA, USA, in June 2010. Fig. 5(a) shows the approximate channel geometry, the structure of the receiver array spanning a total linear aperture of 1.32 m, and the ship trajectory along which the repeated transmission of OFDM signals occurred during 3.5 h of recording. During this time, two sets of OFDM signals, labeled S_1 and S_2 in Fig. 5(b), were transmitted using the acoustic frequency range between 10.5 and 15.5 kHz. The first set S_1 consisted of six frames of ZP-OFDM blocks, which differed in the number of carriers ranging from 64 to 2048. The signals in set S_2 included three superframes corresponding to QPSK ZP-OFDM, QPSK CP-OFDM, and 8-PSK ZP-OFDM blocks. Each superframe consisted of five frames with different number of carriers ranging from 128 to 2048.

Fig. 6(a) shows the structure of the ZP-OFDM frames whose parameters are shown in Table II. Each frame includes a preamble, N_b OFDM blocks consisting of a total of $N_d = 2^{13}$ differentially encoded QPSK or 8-PSK symbols, and a postamble. The synchronization preamble and postamble are short signals formed from a pseudonoise sequence mapped to a unit-amplitude binary PSK alphabet.

Fig. 6(b) shows the block diagram of the receiver used to process the received signals from the MACE'10 experiment. Frame synchronization is performed using the method proposed in [5]. Front-end resampling is then applied to compensate for the time compression/dilation that the received signal experiences. To obtain a rough estimate of Doppler scaling factor, we measure the length of the received frame as $T_{\text{rx}} = T_{\text{tx}} + \Delta\tau$ where T_{tx} is the transmitted frame duration and $\Delta\tau$ represents the amount of time compression/dilation. Time compression/dilation is obtained as $\Delta\tau = \arg\max_\tau |R_{\text{pre,post}}(\tau)|$ where $R_{\text{pre,post}}(\tau)$ is the correlation between the received preamble and postamble signals (its magnitude peaks at lag zero if there is no time compression/dilation). The Doppler scale estimate is given by $\hat{a} = T_{\text{tx}}/T_{\text{rx}} - 1$, and the received signal is resampled accordingly, by a factor $1/(1+\hat{a})$ [12]. Recall that this resampling pertains to an entire frame of blocks, possibly leaving individual blocks within a frame with a different residual frequency offset.

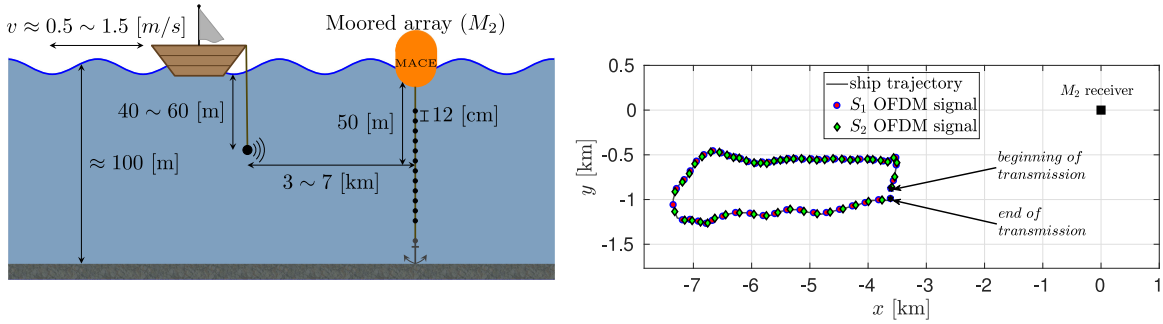

Fig. 5. (a) Channel geometry and receiving array structure of the MACE'10 experiment. (b) Ship trajectory. The transmitter first moved away from the receiver, then toward the receiver at a varying speed that ranged from 0.5 m/s to 1.5 m/s. This process took approximately 3.5 h, during which there were 52 transmissions of S_1 and S_2 signals (small circles and diamonds, respectively) every 4 min. Every odd transmission (S_1) consisted of six frames of ZP-OFDM blocks and each of the frames contained a total of 2^{13} differentially encoded QPSK symbols. In even transmissions (S_2), the transmitted signal consisted of three superframes. The first two superframes each contained five frames of ZP-OFDM and CP-OFDM blocks with a total of 2^{13} differentially encoded QPSK symbols. The last superframe included five frames of ZP-OFDM blocks, each with a total of 2^{13} differentially encoded 8-PSK symbols.

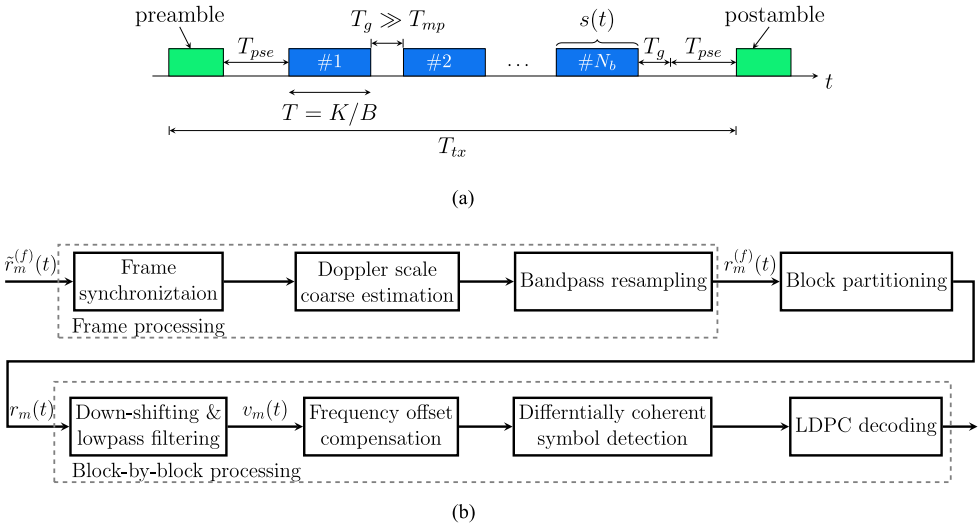

Fig. 6. (a) Illustration of the structure of a sample ZP-OFDM frame. (b) Block diagram of the receiver used in processing the recorded MACE'10 data. The pause interval between the preamble and the OFDM signal is $T_{\text{pse}} = 32$ ms. T_{mp} denotes the delay spread of the channel. Time compression/dilation is estimated as the lag that maximizes the correlation between the received preamble and postamble signals [12].

TABLE II
MACE'10 SIGNAL PARAMETERS

number of carriers K	128	256	512	1024	2048
number of blocks per frame N_b	64	32	16	8	4
carrier spacing Δf [Hz]	39.1	19.5	9.8	4.9	2.4
bit rate [kbps]	9.2	11.4	13	13.9	14.4
bandwidth efficiency [bps/Hz]	1.8	2.3	2.6	2.8	2.9

The guard interval is $T_g = 16$ ms. The total bandwidth is $B = 5$ kHz and the lowest carrier frequency is $f_0 = 10.5$ kHz. The uncoded bit rate and bandwidth efficiency are calculated for 8-PSK modulation. The values of the bit rate and bandwidth efficiency for QPSK modulation are $2/3$ of the corresponding 8-PSK values. The bandwidth efficiency is obtained assuming eight pilots per block.

We demonstrate the performance of the proposed SG algorithm for residual frequency offset compensation in terms of data detection MSE and average execution time $\bar{T}_{\text{exe}}$, which is deemed a practical indicator of the algorithm complexity. We also report on the estimated cumulative density function (CDF) of the MSE measured in each signal frame. Furthermore, we show the BER and block error rate (BLER) of the system when low-density parity check (LDPC) codes are used with various code rates.

The MSE corresponding to an OFDM signal with K carriers is measured in the nth block of the ith frame as follows:

$$\text{MSE}^i(n,K) = \frac{1}{K-1}\sum_{k=1}^{K-1} |b_k^i(n) - \hat{b}_k^i(n)|^2 \qquad (18)$$

and the MSE per frame is obtained as follows:

$$\text{MSE}^i(K) = \frac{1}{N_b}\sum_{n=1}^{N_b} \text{MSE}^i(n,K). \qquad (19)$$

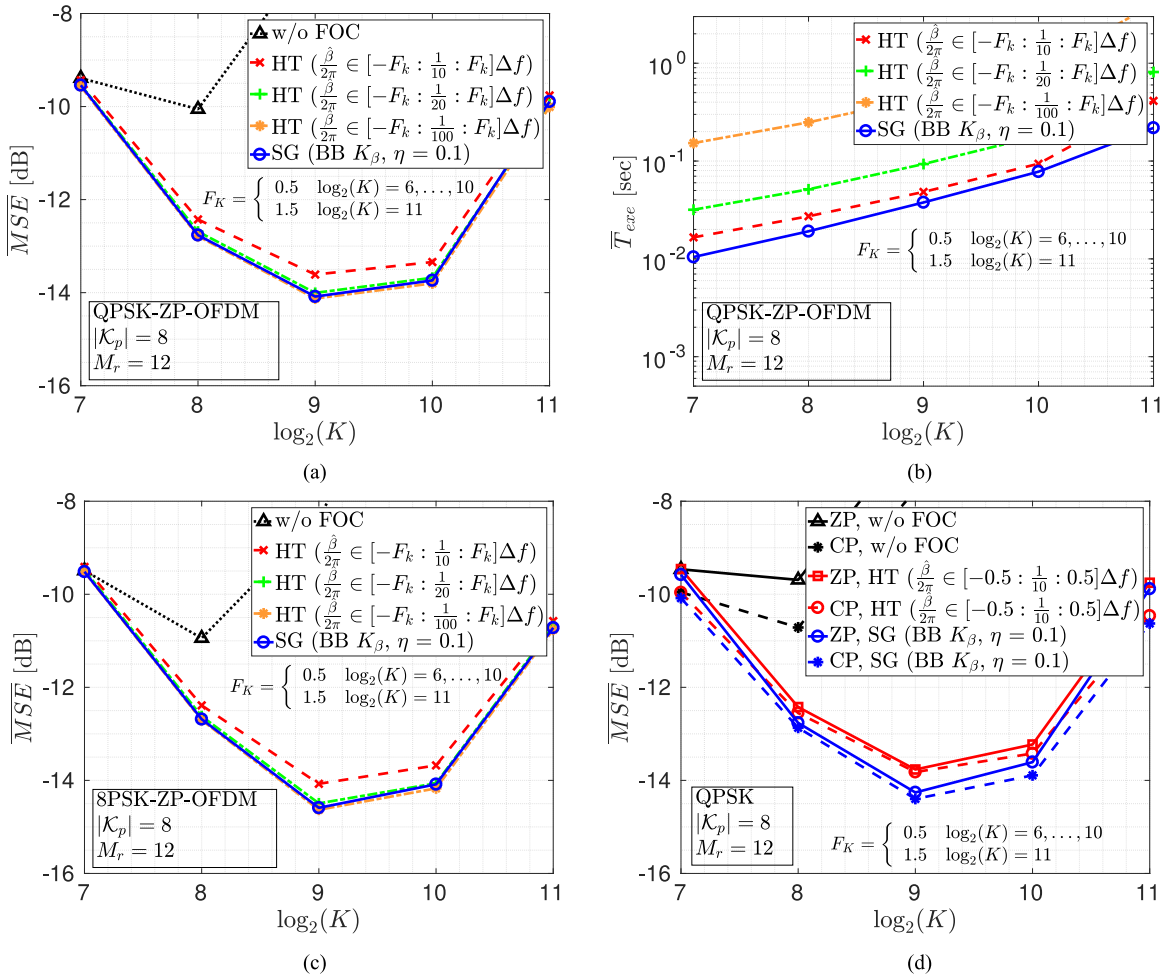

Fig. 7. (a) Average MSE versus the number of carriers K for ZP-OFDM blocks containing differentially encoded QPSK symbols. (b) Average execution time as a function of the number of carriers (log scale). (c) Average MSE as a function of the number of carriers for ZP-OFDM blocks containing differentially encoded 8-PSK symbols. (d) Average MSE versus the number of carriers for ZP-OFDM and CP-OFDM. In (a), (b), and (d), the performance of the systems equipped with the HT and SG algorithms is compared to that of the system without any frequency offset compensation (w/o FOC). The results in (a) and (b) are obtained by averaging over 104 transmissions of ZP-OFDM frames containing QPSK symbols. Each point in (c) and (d) is obtained from 52 transmissions of signals in the set S_2. The HT algorithm is applied to the first block of each frame to initialize the SG algorithm, which then refines the estimate. In (b), the average number of stochastic recursions performed is 3.6, 3.9, 4, 3.7, and 2.8 for $\log_2 K = 7$, 8, 9, 10, and 11, respectively. All 12 receiving elements are used to perform DMRC (6) and only 8 pilots are used to form the composite squared error (7) in each block.

The average over all N_f frames is

$$\overline{\mathrm{MSE}}(K) = \frac{1}{N_f} \sum_{i=1}^{N_f} \mathrm{MSE}^i(K). \tag{20}$$

Note that due to the random channel variation and a finite number of measurements, each of these quantities is a random variable.

Fig. 7 illustrates the average MSE and the average execution time of the HT and SG algorithms as a function of the number of carriers K (log scale). In the SG algorithm, for the first block of each frame, a rough estimate of the frequency offset estimate is first obtained using the HT algorithm with the hypothesis interval $[-3\Delta f, 3\Delta f]$ (acquisition step). The SG algorithm is then applied to obtain a fine estimate of the frequency offset. From the second block and on, only the SG algorithm is used. The initial value of the frequency offset in a current block is set to the frequency offset estimated in the previous block based on the grounds that the frequency offset is not changing significantly from one block to the next. For the HT algorithm, based on the same reasoning, the hypothesis interval $[-3\Delta f, 3\Delta f]$ is changed from the second block and on to shorter intervals $[-F_K \Delta f, F_K \Delta f]$ around the frequency offset estimated in the previous block. $F_K = 0.5$ for K between 64 and 1024, and $F_K = 1.5$ for $K = 2048$, while the resolution factor remains the same as in the first block. To provide a performance bound relevant for the experimental data, the performance of the HT algorithm for larger resolution factors; namely, 20 and 100, is also shown. The exhaustive performance analysis of the HT algorithm can be found in [12]. It is remarkable to see that the SG algorithm achieves the performance bound while incurring a lower computational cost than the HT algorithm. Since increasing the resolution factor from 10 to 20 and 100 does not improve the performance of the HT algorithm significantly, we

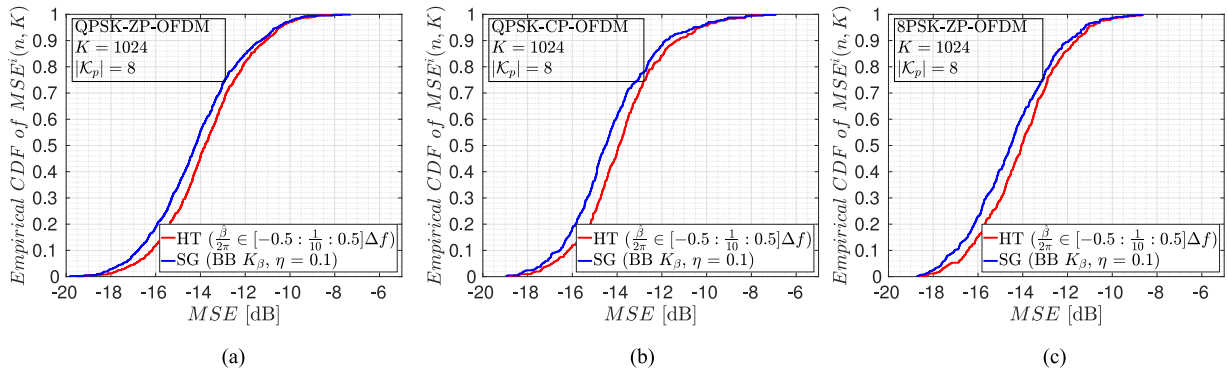

Fig. 8. Estimated CDF of the MSE for the SG and HT algorithms applied to the three configurations of transmitted signals, (a) QPSK ZP-OFD, (b) QPSK CP-OFDM, and (c) 8-PSK ZP-OFDM. The CDFs in (a) reflect all 104 transmissions with $K = 1024$ carriers during MACE'10. The CDFs in (b) and (c) are obtained from 52 transmissions of S_2 signals with the same number of carriers. In (a)–(c), the SG algorithm delivers MSE below -12 dB for 86%, 90%, and 90% of the transmitted OFDM blocks, respectively.

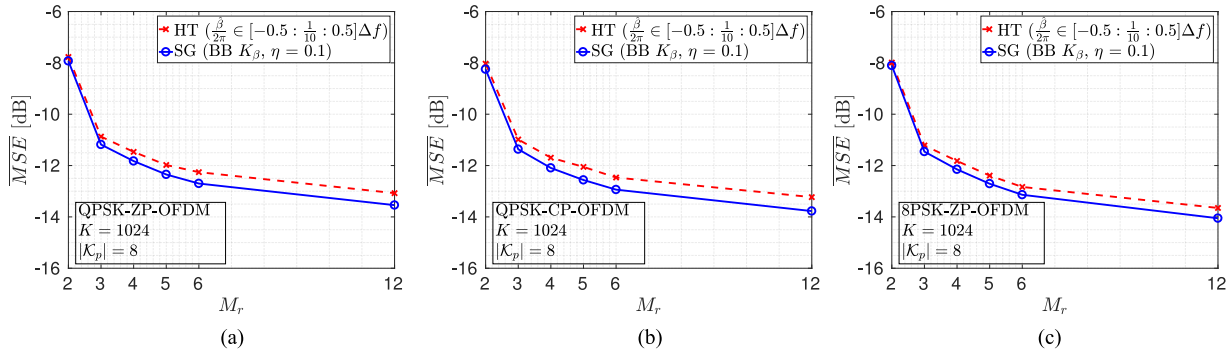

Fig. 9. Average MSE versus the number of receiving elements. The number of carriers and pilots are 1024 and 8, respectively. The receiving elements are maximally spaced. (a) MSE versus M_r for QPSK ZP-OFDM. (b) MSE versus M_r for QPSK CP-OFDM. (c) MSE versus M_r for 8-PSK ZP-OFDM.

set the resolution factor to 10 throughout the rest of analysis. Each point in Fig. 7(a) and (b) is obtained by averaging over all carriers, blocks, and 104 ZP-OFDM frames from the sets S_1 and S_2. Each point in Fig. 7(c) and (d) is obtained from averaging over 52 transmissions of S_2 signals.

Fig. 7 clearly shows that the SG algorithm results in superior performance in terms of the average MSE and average running time. Fig. 7(b) compares the running time of the HT algorithm with the SG algorithm and shows that the SG algorithm has lower complexity than the HT method. It thus enables operation with a greater number of carriers, effectively increasing the bandwidth efficiency at a lower computational complexity. Lower computational complexity and better MSE performance make the SG algorithm a good practical candidate for frequency offset compensation in acoustic OFDM systems. Fig. 7(c) provides the MSE performance for the ZP-OFDM frames containing differentially encoded 8-PSK symbols. Fig. 7(d) illustrates data detection MSE for frames containing ZP-OFDM and CP-OFDM blocks. As expected, CP-OFDM exhibits slightly better performance at the cost of more transmission energy.

Fig. 8 illustrates the estimated CDF of the MSE per block for the three different scenarios (QPSK ZP-OFDM, QPSK CP-OFDM, and 8-PSK ZP-OFDM). This result refers to $K = 1024$ carries and includes all the frames, transmitted over 3.5 h. Systems equipped with the SG and HT algorithm deliver MSE below -12 dB for 90% and 86% of blocks, respectively, for the ZP-OFDM blocks conveying differentially encoded 8-PSK symbols. The same performance is observed for the CP-OFDM signals conveying differentially encoded QPSK symbols.

Fig. 9 illustrates the MSE performance as a function of the number of receiving elements M_r, which are chosen maximally and equally spaced among the 12 available elements. Evidently, a significant improvement is observed as the number of elements increases and spatial diversity gain is extracted. Although the best performance (-14 dB of MSE) is achieved by using all the 12 elements, using six elements also provides an excellent performance (-13 dB of MSE). Increasing the number of elements exhibits the effect of diminishing returns as the total array aperture remains the same.

In Fig. 10, we demonstrate the performance of the system used for the three configurations of signals in terms of average BER and average BLER using regular LDPC codes with various code rates ranging from 0.1 to 1. The codeword length is $N = 2K$ for QPSK or $N = 3K$ for 8-PSK, respectively; thus, each codeword constitutes an OFDM block. The column weight of the $M \times N$ parity check matrix, where M is the number of parity bits, is $w_c = 3$ for all the code rates considered, and the row weight $w_r = w_c N/M$ varies from 3.3 to 30 corresponding

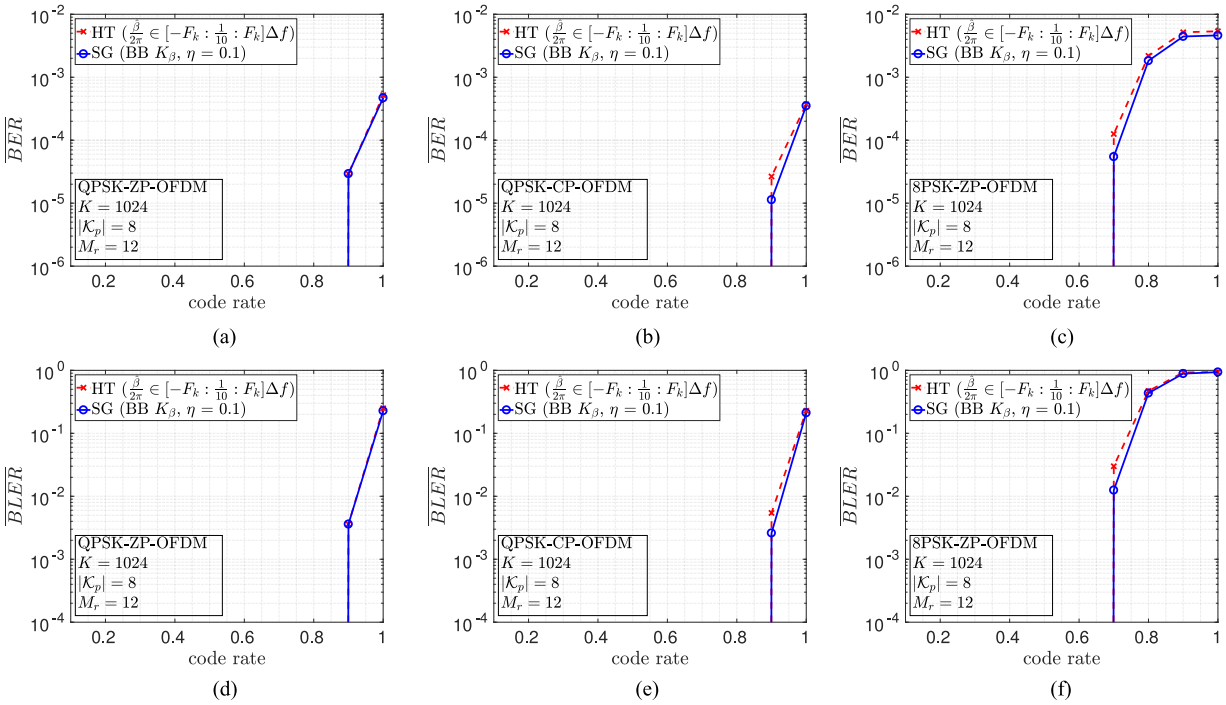

Fig. 10. Top: Average BER versus the rate of the LDPC code. Bottom: Average BLER as a function of rate of the LDPC code. The results in (a) and (d) reflect all 104 transmissions with 1024 carriers during MACE'10. Using code rates as high as 0.9, the frequency synchronization method based on the SG approach enables excellent performance with BER $= 10^{-5}$ and BLER $= 2.4 \times 10^{-3}$ for CP-OFDM blocks. The SG algorithm can also achieve BER and BLER as low as 5.5×10^{-5} and 1.2×10^{-2} for OFDM blocks whose carriers are 8-PSK modulated. (a) BER for QPSK ZP-OFDM. (b) BER for QPSK CP-OFDM. (c) BER for 8-PSK ZP-OFDM. (d) BLER for QPSK ZP-OFDM. (e) BLER for QPSK CP-OFDM. (f) BLER for 8-PSK ZP-OFDM.

to code rates from 0.1 to 0.9 [18]. We use soft decision decoding that takes the likelihood ratio for each code-bit as an input. Decoding is performed based on the probability propagation algorithm that can be seen as an instance of the sum–product algorithm [19]. Employing the proposed algorithms for frequency offset compensation enables LDPC to work to its full potential. Using the SG algorithm and code rate as high as 0.9, we achieve BER and BLER as low as 10^{-5} and 2.4×10^{-3}, respectively, for CP-OFDM frames containing differentially encoded QPSK symbols. Code rates below 0.9 result in low BER values that cannot be measured with the existing data.

VI. Conclusion

We considered differentially coherent detection of acoustic OFDM signals and targeted frequency offset through two methods, HT and SG algorithm, for channels with severe Doppler distortion where random, time-varying frequency shifts can be comparable with the carrier spacing. These methods find the frequency offset by minimizing the squared error of estimated data symbols on only a few pilots. In the HT method, the frequency offset estimate is found through a simple linear search over an interval of hypothesized values with a prespecified resolution. In contrast, the SG algorithm yields an estimate of the frequency offset with superresolution. The convergence speed of the SG algorithm can be improved by coupling it with the HT, which acts as an acquisition technique with no constraint on the acquisition range. These techniques can be used as a stand-alone approach for differentially coherent detection, but they can also be employed as a preprocessing stage for coherent detection. The key feature is that only a few pilots suffice to determine the frequency shift, and once the frequency offset has been compensated, data symbols can be detected either in a coherent or differentially coherent manner.

We presented a statistical performance analysis using both simulation and experimental data recorded over a mobile acoustic channel. Simulation results, as well as experimental results obtained using the MACE'10 data, clearly show the effectiveness of the SG algorithm in compensating for the motion-induced time variation of the channel. Specifically, excellent performance was achieved with real data using 12 receiving elements, and up to 2048 carriers which convey differentially encoded QPSK/8-PSK data symbols and occupy the acoustic frequency range between 10.5 and 15.5 kHz, corresponding to the transmission rate of 14.4 kb/s (13 kb/s if with rate 0.9 LDPC). The average MSE observed over 25 800 transmitted OFDM blocks during the MACE'10 is -12 dB. Our results show that the proposed method delivers an average MSE below -12 dB for 90% of OFDM blocks and enables a very high rate LDPC code to achieve an excellent BER of 10^{-5} and BLER of 2.4×10^{-3} at very low computational complexity.

In addition to providing excellent performance, the proposed method enables operation with a greater number of carriers, thus increasing the bandwidth utilization with minimum pilot overhead. Most notably, the running time of the SG algorithm is much smaller than the duration of OFDM symbol (e.g., the

running time of SG algorithm is three times shorter than the duration of an OFDM symbol with $K = 1024$ carriers), thus offering an appealing solution for real-time implementation in high-rate, mobile UWA systems.

REFERENCES

[1] M. Stojanovic, "Low complexity OFDM detector for underwater acoustic channels," in *Proc. OCEANS Conf.*, Boston, MA, USA, Sep. 2006, pp. 1–6.

[2] M. Stojanovic, "OFDM for underwater acoustic communications: Adaptive synchronization and sparse channel estimation," in *Proc. IEEE Int. Conf. Acoust., Speech Signal Process.*, Las Vegas, NV, USA, 2008, pp. 5288–5291.

[3] B. Li, S. Zhou, M. Stojanovic, L. Freitag, and P. Willett, "Multicarrier communication over underwater acoustic channels with nonuniform Doppler shifts," *IEEE J. Ocean. Eng.*, vol. 33, no. 2, pp. 198–209, Apr. 2008.

[4] K. Tu, T. M. Duman, M. Stojanovic, and J. G. Proakis, "Multiple-resampling receiver design for OFDM over Doppler-distorted underwater acoustic channels," *IEEE J. Ocean. Eng.*, vol. 38, no. 2, pp. 333–346, Apr. 2013.

[5] Y. M. Aval and M. Stojanovic, "Differentially coherent multichannel detection of acoustic OFDM signals," *IEEE J. Ocean. Eng.*, vol. 40, no. 2, pp. 251–268, Apr. 2015.

[6] T. Pollet, M. Van Bladel, and M. Moeneclaey, "BER sensitivity of OFDM systems to carrier frequency offset and Wiener phase noise," *IEEE Trans. Commun.*, vol. 43, no. 234, pp. 191–193, Feb.–Apr. 1995.

[7] P. H. Moose, "A technique for orthogonal frequency division multiplexing frequency offset correction," *IEEE Trans. Commun.*, vol. 42, no. 10, pp. 2908–2914, Oct. 1994.

[8] T. M. Schmidl and D. C. Cox, "Robust frequency and timing synchronization for OFDM," *IEEE Trans. Commun.*, vol. 45, no. 12, pp. 1613–1621, Dec. 1997.

[9] J.-J. Van de Beek, M. Sandell, and P. O. Borjesson, "ML estimation of time and frequency offset in OFDM systems," *IEEE Trans. Signal Process.*, vol. 45, no. 7, pp. 1800–1805, Jul. 1997.

[10] A. Masoomzadeh-Fard and S. Pasupathy, "Nonlinear equalization of multipath fading channels with noncoherent demodulation," *IEEE J. Sel. Areas Commun.*, vol. 14, no. 3, pp. 512–520, Apr. 1996.

[11] M. Stojanovic, "An adaptive algorithm for differentially coherent detection in the presence of intersymbol interference," *IEEE J. Sel. Areas Commun.*, vol. 23, no. 9, pp. 1884–1890, Sep. 2005.

[12] A. Tadayon and M. Stojanovic, "Frequency offset compensation for acoustic OFDM systems," in *Proc. OCEANS Conf.*, Anchorage, AK, USA, 2017, pp. 1–5.

[13] B. Muquet, Z. Wang, G. B. Giannakis, M. de Courville, and P. Duhamel, "Cyclic prefixing or zero padding for wireless multicarrier transmissions?" *IEEE Trans. Commun.*, vol. 50, no. 12, pp. 2136–2148, Dec. 2002.

[14] D. Rife and R. Boorstyn, "Single tone parameter estimation from discrete-time observations," *IEEE Trans. Inf. Theory*, vol. IT-20, no. 5, pp. 591–598, Sep. 1974.

[15] B. Mamandipoor, D. Ramasamy, and U. Madhow, "Newtonized orthogonal matching pursuit: Frequency estimation over the continuum," *IEEE Trans. Signal Process.*, vol. 64, no. 19, pp. 5066–5081, Oct. 2016.

[16] J. Barzilai and J. M. Borwein, "Two-point step size gradient methods," *IMA J. Numer. Anal.*, vol. 8, no. 1, pp. 141–148, 1988.

[17] P. Qarabaqi and M. Stojanovic, "Statistical characterization and computationally efficient modeling of a class of underwater acoustic communication channels," *IEEE J. Ocean. Eng.*, vol. 38, no. 4, pp. 701–717, Oct. 2013.

[18] W. Ryan and S. Lin, *Channel Codes: Classical and Modern*. Cambridge, U.K.: Cambridge Univ. Press, 2009, pp. 201–202.

[19] D. J. MacKay, "Good error-correcting codes based on very sparse matrices," *IEEE Trans. Inf. Theory*, vol. 45, no. 2, pp. 399–431, Mar. 1999.

Amir Tadayon (S'07–GS'15) received the B.S. degree in electrical engineering from Tehran University, Tehran, Iran, in 2011, and the M.S. degree in electrical engineering from Northeastern University, Boston, MA, USA, in 2016; where he is currently working toward the Ph.D. degree in electrical engineering.

His research interests include statistical signal processing and digital communications, and their applications to underwater acoustic systems.

Milica Stojanovic (SM'08–F'10) received the Dipl.Ing. in electrical engineering from the University of Belgrade, Belgrade, Serbia, in 1988, and the M.S. and Ph.D. degrees in electrical engineering from Northeastern University, Boston, MA, USA, in 1991 and 1993, respectively.

She was a Principal Scientist at the Massachusetts Institute of Technology, Cambridge, MA, USA and in 2008, she joined Northeastern University, where she is currently a Professor of Electrical and Computer Engineering. She is also a Guest Investigator with the Woods Hole Oceanographic Institution, Woods Hole, MA, USA. Her research interests include digital communications theory, statistical signal processing, and wireless networks, and their applications to underwater acoustic systems.

Prof. Stojanovic is the recipient of the 2015 IEEE/OES Distinguished Technical Achievement Award, and is the 2008 IEEE/OES Distinguished Lecturer. She is an Associate Editor for the IEEE JOURNAL OF OCEANIC ENGINEERING and a Past Associate Editor for the IEEE TRANSACTIONS ON SIGNAL PROCESSING and the IEEE TRANSACTIONS ON VEHICULAR TECHNOLOGY. She also serves on the Advisory Board of the IEEE COMMUNICATIONS LETTERS and the Editorial Board of IEEE SIGNAL PROCESSING MAGAZINE, and Chairs of the IEEE Ocean Engineering Society's Technical Committee for Underwater Communication, Navigation, and Positioning.